



CHORUS

This is the accepted manuscript made available via CHORUS. The article has been published as:

Gate-Tunable Landau Level Filling and Spectroscopy in Coupled Massive and Massless Electron Systems

Bin Cheng, Yong Wu, Peng Wang, Cheng Pan, T. Taniguchi, K. Watanabe, and M. Bockrath

Phys. Rev. Lett. **117**, 026601 — Published 8 July 2016

DOI: [10.1103/PhysRevLett.117.026601](https://doi.org/10.1103/PhysRevLett.117.026601)

Gate-Tunable Landau Level Filling and Spectroscopy in Coupled Massive and Massless Electron Systems

Bin Cheng,¹ Yong Wu,¹ Peng Wang,¹ Cheng Pan,¹ T. Taniguchi,² K. Watanabe,² M. Bockrath¹†

¹Department of Physics and Astronomy, University of California, Riverside, California 92521, USA.

²Advanced Materials Laboratory, National Institute for Materials Science, Tsukuba, Ibaraki 305-0044, Japan.

†Correspondence and requests for materials should be addressed to M. B. (marc.bockrath@ucr.edu)

We report transport studies on coupled massive and massless electron systems, realized using twisted monolayer graphene/natural bilayer graphene stacks. We incorporate the layers in a dual-gated transistor geometry enabling independently tuning their charge density and the perpendicular electric field. In a perpendicular magnetic field, we observe a distinct pattern of gate-tunable Landau level crossings. Screening and interlayer electron-electron interactions yield a nonlinear monolayer gate capacitance. Data analysis enables determination of the monolayer's Fermi velocity and the bilayer's effective mass. The mass obtained is larger than that expected for isolated bilayers, suggesting that the interlayer interactions renormalize the band structure.

Placing two-dimensional (2D) material layers in close proximity with a twist angle yields material systems with new properties [1-13]. For example, at small twist angles the moiré superlattice enables the investigation of Hofstadter butterfly physics [14-18] or momentum-conserved tunneling [1, 7]. Moreover, charge screening of closely spaced layers, which depends crucially on the strong interlayer electron-electron interactions and their electronic quasiparticle spectra, influences the system properties [19-22]. In particular, an interesting situation arises in a twisted graphene trilayer (TTL) [11-13], where a graphene monolayer (massless spectrum) [23] is stacked onto and interacts with a graphene bilayer (massive spectrum) [23]. Band structure and optical property changes have been predicted with twist angle [11, 12]. However, interacting-electron phenomena such as screening and interlayer interactions that are important to the behavior of realistic systems remain unaddressed.

Here we study TTLs via transport measurements under perpendicular magnetic and electric fields. Unlike prior works on natural ABA-stacked trilayers [24-28], we couple the different spectrum layers to independent electrostatic gates, enabling independent tuning of the charge density in the system and the interlayer potential difference. We find that because of charge screening, the monolayer gate capacitance is strongly nonlinear, with its charge increasing approximately quadratically with gate voltages. Furthermore, we demonstrate tunable interlayer Landau level (LL) crossings by varying both gate voltages. The crossing pattern is modified at the charge neutrality point (CNP) of the bilayer when a nonzero electric field across the bilayer opens a band gap [23], resulting from the electrostatic potential shift required to tune the bilayer from electron to hole doping. From the estimated interlayer capacitance, we simultaneously determine the electronic Fermi velocity v_F within the monolayer and effective mass m in the bilayer, as well as LL spectrum for each layer of the TTL for the first time. Significant v_F renormalization was not observed, consistent with ref. [13] in twisted bilayers at large twist angles. However, we find a significantly larger estimated m than in isolated bilayers, suggesting

that the interlayer interaction can renormalize the TTL layers' band structure, similar to the behavior reported previously for twisted bilayer stacks [29], although the magnitude of the renormalization we observe is much larger in the TTL system.

The devices consist of an hBN-encapsulated TTL stack. Figure 1(a) shows the device geometry and capacitances C_i , C_b , and C_t , which are the geometric interlayer, bottom and top gate capacitances per unit area, respectively, and the tunnel junction between the bilayer and monolayer. The stack is etched and contacted in a Hall bar geometry that enables measurement of the longitudinal resistance R_{xx} and the Hall resistance R_{xy} [30]. The top metal gate and bottom Si gate independently tune the total charge density and the perpendicular electric field on the two layers. A measurement of R_{xx} is shown in the color plot in Fig. 1(b) inset vs. the top gate voltage V_{ig} and the bottom gate voltage V_{bg} . The bright line is a resistance maximum for each gate trace. Line traces of the 4-terminal $R_{xx}(V_{bg})$ are shown in the Fig. 1(b) main panel, taken at a temperature $T=1.5$ K. The resistivity shows a maximum at $V_{ig}=2$ V and $V_{bg}=-20$ V. For the large twist angle and weak tunnel coupling in our devices the bilayer and monolayer graphene can be considered as parallel resistors, similar to twisted bilayers [19]. Both the bilayer and monolayer have their resistivity maximum at the CNP, and the linear bright region in the Fig. 1(b) inset occurs near total charge neutrality summed over both layers where the parallel combination of resistances is maximized, while the largest R_{xx} maximum shown in Fig. 1(b) corresponds approximately to both layers being simultaneously charge neutral.

In a perpendicular magnetic field B , LLs form in the two layers' energy spectra [23]. However, because the bilayer's quasiparticles are massive while the monolayer's are massless, their spectra are very different. The bilayer LL energies for index l are $\epsilon_l = \hbar\omega_c + \epsilon_{l0}$, where $\omega_c = eB/m$ is the cyclotron frequency, e is the electric charge, \hbar is Planck's reduced constant, and m the effective mass of carriers. The zero energy LL is eightfold degenerate, whereas higher $l > 1$ levels are fourfold degenerate [23]. In contrast, the monolayer LL energies are $\epsilon_l = \hbar\omega_c$, with all levels fourfold degenerate [23]. The LL degeneracies in the mono- and bilayers can be lifted by symmetry breaking perturbations such as electron-electron interactions or environmental coupling [31, 32].

To investigate LL filling in the two coupled layers, we measure R_{xx} versus V_{ig} and V_{bg} at $B=8$ T [Figure 2(a)]. Linear minima features, such as those indicated by the black arrows, correspond to spectral gaps between LLs, while bright features present within the gaps such as those marked by the black dots are associated with steps in the Hall conductance of $8e^2/h$, where h is Planck's constant [30], indicating that these correspond to LL crossings or inter-LL transitions.[19] Shallower minima also occur, indicating symmetry breaking perturbations and the lifting of the LL degeneracies [31, 32]. The bilayer $l=0,1$ states are shown between the two arrows, where the density changes by 8 LLs between the prominent gap features, with the line trace shown in the Fig. 2(a) inset. In Fig. 2(a), straight lines connecting LL degeneracy points at constant bilayer charge, such as those marked by the blue dashed lines, are uniformly spaced. In contrast, crossing points at constant monolayer charge, such as those marked by the red dashed lines, are spaced non-uniformly, with the largest spacing at low doping. This shows that the gate capacitance to the monolayer is nonlinear while the bilayer gate capacitance appears to be linear.

To understand this behavior, each layers' band structure is assumed to be that of the isolated layers due to weak tunnel coupling (although with possibly renormalized parameters) [11]. Since the bilayer LL energies are $\propto B$, while those of the monolayer are $\propto B^{1/2}$, monolayer or bilayer LL states will tend to preferentially fill depending on which has the smaller level spacing near the Fermi level. Considering interactions, electrons are subject to interlayer repulsion and gate charge screening. The latter depends on the interactions of electrons within the same layer. This screening is imperfect, which leads to quantum corrections to the capacitance [22, 33-37]. These effects are expected to strongly affect the LL filling behavior and layer capacitance. Moreover, because of the imperfect screening, an electric field can exist between the two layers, yielding an electrostatic potential difference between them.

However, at equilibrium, the two layers' electrochemical potentials, which are the sum of the electrostatic and chemical potentials within the layers, are expected to be equal and are at the ground potential of the circuit. With these assumptions, the expected slopes $\Delta V_{tg}/\Delta V_{bg}$ connecting the major features in the data in the V_{bg} - V_{tg} plane can be determined by equating two different expressions for the charge density on each layer. One is determined from the electrostatic potentials across the capacitances in the circuit. The other is obtained from the electrostatic potentials in each layer using a Thomas-Fermi model and their density of states[23] yielding:

$$C_i(\phi_b - \phi_m) + C_b(\phi_b - V_{bg}) = -\frac{2me^2\phi_b}{\pi\hbar^2} \quad (1)$$

$$C_i(\phi_m - \phi_b) + C_t(\phi_m - V_{tg}) = \frac{\sigma e^3 \phi_m^2}{\pi\hbar^2 v_F^2}. \quad (2)$$

Here, ϕ_m (ϕ_b) is the electrostatic potential of the monolayer (bilayer), and σ determines the sign of the charge density in the monolayer. Solving these equations for ϕ_m and ϕ_b enables determination of the charge densities in the two layers and the constant charge condition for each layer versus V_{tg} and V_{bg} . We also assume that the electrostatic potentials of the gate electrodes are equal to their applied voltages, neglecting quantum capacitance corrections for C_t and C_b . We focus on three predominant slopes in the V_{tg} - V_{bg} plane, those connecting crossing points at constant monolayer charge, m_{cmc} , constant bilayer charge m_{cbc} , and constant total charge, m_c . Using eqs. 1 and 2 we find, to a good approximation, $m_c = -C_b/C_t$. [30] and obtain $m_c = -0.089$ from the Fig. 2(a) data. From the measured V_{bg} spacing between successive R_{xx} dips at $B=8$ T, we find $C_b = 1.0 \times 10^{-4}$ F/m², and $C_t = -C_b/m_c = 1.2 \times 10^{-3}$ F/m². Measuring the slope along the dashed red lines in Fig. 2(a) gives $m_{cmc} = -0.037$, while the slope along the blue dashed lines gives $m_{cbc} = -0.14$. Also from eqs 1. and 2 we find $m_{cmc} = -\alpha C_i C_b / C_t$ [30], where α is a constant given by $\alpha \approx [C_i + 2me^2/(\pi\hbar^2)]^{-1}$ [30]. By using this equation for m_{cmc} and its measured value we determine the dimensionless product $\alpha C_i = 0.41$.

To find C_i and α independently and determine m , we plot in Fig. 2(b) R_{xx} versus total electron density n and the total displacement field $D = 1/2(C_b V_{bg} - C_t V_{tg})$ applied to all the layers. At constant n , D tunes the bilayer-monolayer interlayer potential $\Delta\phi$ such that $\Delta\phi = d_i D / \epsilon_i = D / C_i$, where d_i is the interlayer spacing, and ϵ_i is the interlayer dielectric constant[19]. When $D \neq 0$, the displacement field across the bilayer $D_{b\perp}$ opens a band gap within it E_g [23, 38].

We determine C_i from the change in D necessary to tune the monolayer zeroth LLs through the gap ($\equiv \Delta D_{gap}$), using $\Delta\phi = E_g/e = \Delta D_{gap}/C_i$, and obtaining E_g from $D_{b\perp}$ based on previous bilayer measurements [23]. We first find the gate voltage conditions yielding $E_g = 0$ and $D_{b\perp} = 0$, using the degeneracy at bilayer filling factor $\nu_b = -3$ occurring when $D_{b\perp} = 0$ [39], which produces the peak in the red curve in Fig. 2(c). We next determine ΔD_{gap} by finding the change in D necessary to tune the monolayer 0th LL states through the bilayer gap. The alignment between the monolayer 0th LL states and bilayer valence band states occurs along the black curve in Fig. 2(c) [taken along the black dashed line in Fig. 2(b)], at the rightmost of four peaks, with the corresponding alignment shown in Fig. 2(d) (alignment A). [The other three peaks are produced by LL crossings shown in Fig. 2(e).] The black arrow in Fig. 2(b) marks where the lowest zeroth LL monolayer (cyan dotted line) and bilayer electron states (green dotted line) align [alignment B, Fig 2(f)]. The ΔD_{gap} to tune between the A and B alignments is $\Delta D_{gap} \approx 140$ mV/nm [Fig. 2(c)]. The magnitude of E_g is determined by $\Delta D_{b\perp} \approx 250$ mV/nm, measuring from $D_{b\perp} = 0$ to the midpoint between the two leftmost dashed lines to account for the increase of E_g as D increases. From $\Delta D_{b\perp}$ we determine $E_g \approx 20$ meV from previous literature [40, 41]. Using $E_g/e = \Delta D_{gap}/C_i$ we find $C_i = 0.062$ F/m². This is approximately a factor of two larger than the value obtained by a parallel

plate model for the two layers, suggesting a relative interlayer dielectric constant ~ 2 . From this we find $m=0.065m_e$, where m_e is the free electron mass.

To investigate LL filling in both layers as B and the gate voltages vary, Fig. 3(a) shows R_{xx} versus B and V_{bg} with V_{tg} continuously adjusted so that $D=0$. The LL crossings are identified as bright regions in the data where R_{xx} dips at constant total filling factor are suppressed, such as that marked by the arrow. Changing V_{tg} so that $D \neq 0$ tunes the filling pattern, as shown in Fig. 3(b), which shows data with $V_{tg}=V_{bg}/4 \times C_b/C_t$ having sparser crossing points.

To understand this behavior we consider that although the closest gate to each layer dominantly affects its charge, due to imperfect screening each gate affects both layers' charge. Using eqs. 1 and 2 we find V_{bg} corresponding to the crossing points for appropriate integer monolayer filling factors $\nu > 0$ as:

$$C_0 V_{bg} = \alpha C_i m v_F \left(\frac{2B \nu e^3}{\hbar^3} \right)^{1/2} + \frac{e^2 B \nu}{2\hbar}, \quad (3)$$

where $C_0 = \pi(\alpha C_i C_b + C_t \beta)$ and V_{tg} is assumed to be maintained such that $V_{tg} = \beta V_{bg}$, with β a constant [30]. The V_{bg} corresponding to the crossing points consists of one term proportional to $m v_F$, and another independent of band structure parameters. For $D=0$, $\beta = C_b/C_t$. The gate voltages of the crossing points for this case is plotted for different values of ν in Fig. 3(c). A fit to the data using this equation yields a value for the product $m v_F \approx 6 \times 10^{26}$ kg·m/s, without requiring direct knowledge of C_i . This gives $v_F \sim 1 \times 10^6$ m/s for all the curves, using the previously determined m . This v_F value agrees well with the value found in previous work [23], with the renormalization expected to be small due to the large twist angle. However, as determining m and v_F independently of their product $m v_F$ requires estimation of C_i , these independent values can be considered only estimates. This is because the result for an isolated bilayer's E_g dependence on D was used to estimate C_i . Nevertheless, the analysis suggests that the interlayer interaction renormalizes the layers' band structure, as the measured product $m v_F$ is larger than that of isolated layers. As previous work has shown that electron-electron interactions renormalize the Fermi velocity in graphene monolayers [42], the strong interlayer electronic interactions could cause a similar renormalization in the TTL. Additionally, theoretical calculations based on non-interacting electrons in the lower symmetry lattice of the twisted layers [11] indicate that both v_F and m tend towards their isolated layer values when the angle becomes larger, while v_F gets smaller and m gets larger as the twist angle approaches zero. In our study, the angle is unknown, although the absence of secondary resistance peaks suggest the angle is $> 1^\circ$. Therefore, a comprehensive understanding of this phenomenon will require future work, for example in conjunction with STM experiments to measure the twist angle, as well as theoretical work to understand the influence of interactions on this system.

Putting $\beta = 1/4 \times C_b/C_t$ into eq. 3 shows that the voltage scales for the LL crossings increase compared to when $D=0$, as observed. In addition, rearranging this equation indicates that the monolayer charge is approximately quadratic in the gate voltages over the gate voltage ranges studied. This accounts for the non-uniform spacing of the features corresponding to LL crossings at fixed monolayer charge indicated by the red dashed lines in Fig. 2(a). In contrast, for the bilayer its nearly constant density of states yields a more linear capacitance for the gate voltage ranges studied [30].

Finally, we see that along the lines of crossing points with constant monolayer charge, some expected crossing points appear to be absent, for example at the point marked by the open circle in the lower portion of Fig. 2(b). This is illustrated in Fig. 4(a), which shows several line traces each at constant density with total filling factor $\nu_T = 10, 6,$ and 2 taken along the vertical white dotted lines in Fig. 2(b). The corresponding level crossing diagram is shown in Fig. 4(b). While two regions of enhanced R_{xx} corresponding to crossing points are visible in the lowest curve [Figs. 4(a-b), green solid square and purple solid triangle] the center curve has only one [Figs. 4(a-b), red solid square], and the

top curve has zero. For the top curve, this occurs because the bilayer electrostatic potential must change by E_g/e to tune the Fermi level across the gap. As a result, the crossing points are displaced, so that when D is tuned to an expected crossing point the situation is as shown in Fig. 4(a-b) by the open blue squares, which accounts for the missing peak. For the center curve, a similar situation arises [Fig. 4(a-b), open red circles]. These points are also labeled by the corresponding symbols in Fig. 2(b). Similar behavior is also observable for hole doping [30]. Finally, we note that the ML 0th LLs cross the BL states without significant displacement because the bilayer band gap is relatively small at the crossing point [Fig. 4(b)].

In sum, using the novel TTL dual-gated structure, we are able to tune the interlayer LL filling rates by varying the voltages on the dual gates. Also, because of screening the total capacitance of the monolayer including quantum capacitance corrections is strongly nonlinear, exhibiting a quadratic dependence of its charge on the gate voltages. On the other hand, the bilayer capacitance is observed to be more linear. Data analysis enables energy spectroscopy of the monolayer and bilayer Landau levels, indicating that the spectrum is renormalized by the interlayer interaction. In future work, placing 2D systems in close proximity to systems with a known spectrum, such as graphene bilayers, may enable detailed investigation of their electronic structure and interactions.

Acknowledgements

B. C. and Y. W. contributed equally to this work. We thank C. N Lau for helpful discussions. B. C., Y. W., and P. W were supported by DOE ER 46940-DE-SC0010597. Additional support for this work was from NSF-DMR-1106358, ONR/DMEA-H94003-10-2-1003 and the UCR CONSEPT Center. This material is based on research sponsored by the Defense Microelectronics Activity (DMEA) under agreement number H94003-10-2-1003. The United States Government is authorized to reproduce and distribute reprints for Government purposes, notwithstanding any copyright notation thereon.

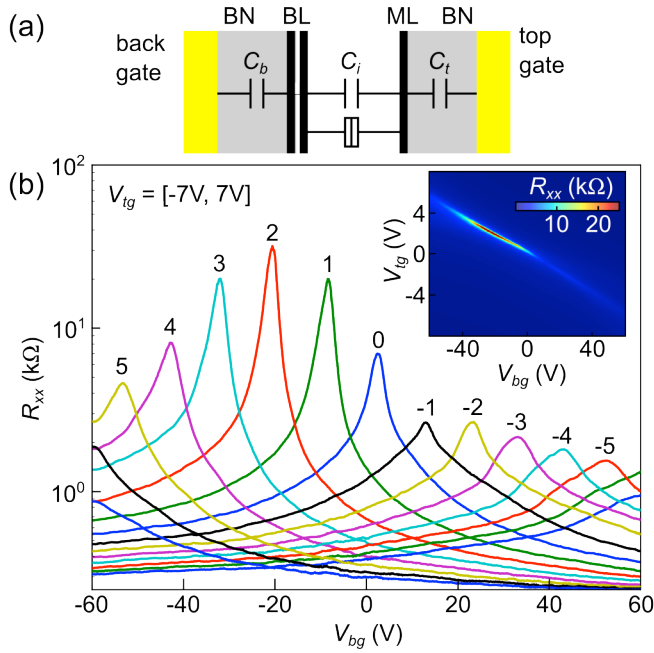


FIG. 1 Device geometry and $B=0$ transport data. (a) Schematic diagram of layer stack showing effective circuit of capacitances and tunnel junction. BL, bilayer graphene, ML monolayer graphene. (b) Inset: $R_{xx}(V_{bg}, V_{tg})$ at $B=0$. The bright linear feature is the charge neutrality line where the total charge carrier density is zero. Main panel: Line cuts $R_{xx}(V_{bg})$ at V_{tg} ranging from -7 V to 7 V. The numbers indicate V_{tg} values in volts.

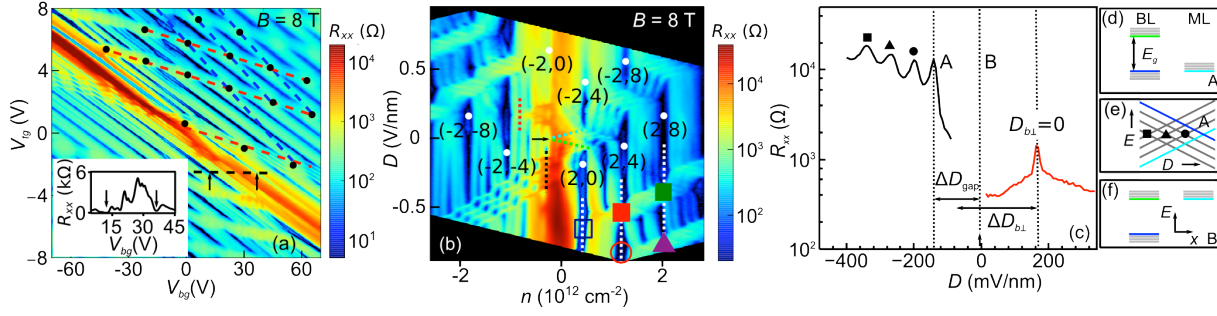


FIG. 2 Magnetotransport data. (a) $R_{xx}(V_{bg}, V_{tg})$ at $B=8$ T. The red (blue) dashed line connects crossing point features for which the monolayer (bilayer) charge is constant. Inset: Plot of R_{xx} taken along the dashed black line in the main panel. The arrows mark minima at $v_b=\pm 4$ (b) $R_{xx}(n, D)$ at $B=8$ T. The LL gaps are labeled by (j, k) , where j (k) is the ML (BL) LL filling factor. (c) Line traces along the red and black dotted lines in (b) with corresponding colors. The rightmost vertical dotted line corresponds to $D_{b\perp}=0$. (d) Schematic energy diagram of level alignments at D value labeled by A and marked by leftmost vertical dotted line in (c). The fourfold energy splitting of the states is indicated schematically. All the states are shown in gray except the uppermost hole-like bilayer state (blue), the lowermost bilayer electron-like state (green) and the lowest energy monolayer state (cyan). (e) Schematic energy (E) diagram of level crossings vs. D near the alignment in (d) using the same color labeling. Crossings corresponding to the three leftmost peaks in the black curve of (c) are labeled by the corresponding black circles, triangles and squares. (f) Same as in (d) but for the B alignment labeled by B.

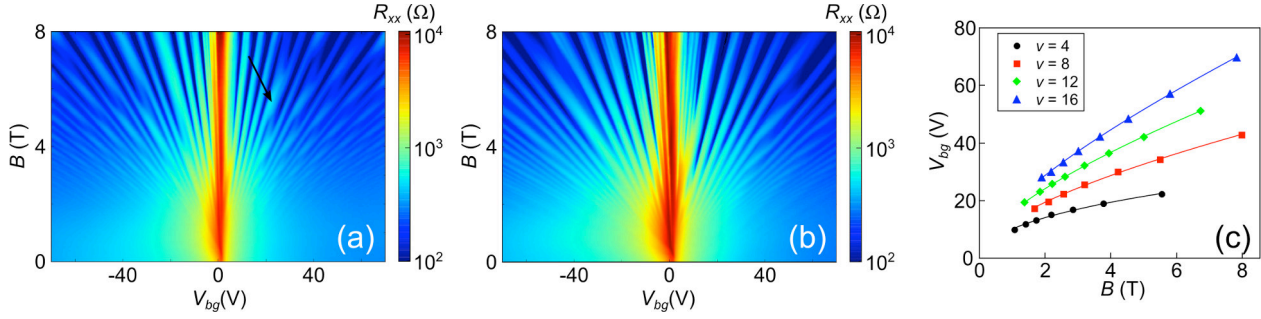


FIG. 3 Gate-tunable Landau level crossings. (a) $R_{xx}(V_{bg}, B)$, where the top gate is adjusted to maintain $D=0$. The arrow indicates a LL crossing point. (b) Similar plot as in (a), but with the ratio V_{tg}/V_{bg} maintained at $0.25 \times C_b/C_t$. The crossing points are sparser than in (a). (c) The gate voltage of the crossing points from (a) is plotted for a number of different values of ν . The Fermi velocities obtained from the fits are $1.2, 1.0, 0.9$ and 0.9×10^6 m/s for $\nu=4, 8, 12$ and 16 , respectively.

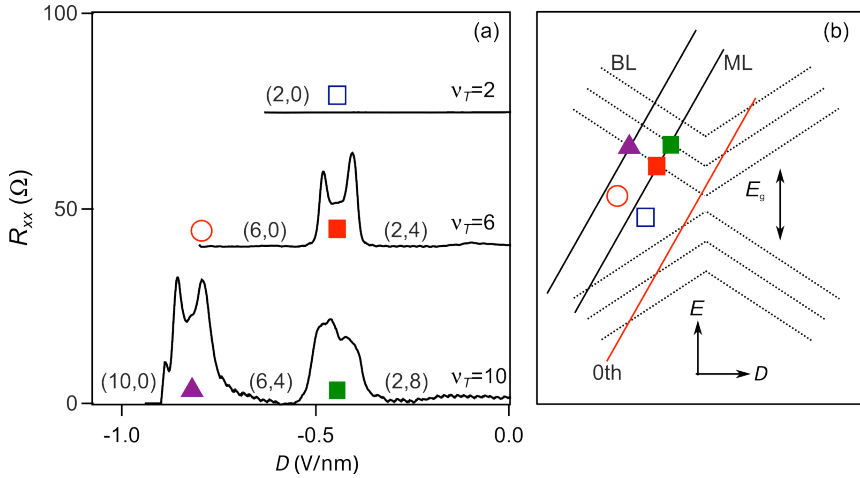


FIG. 4 (a) R_{xx} line traces vs. D for different total filling factors. Plot of R_{xx} vs. D for total filling factors $\nu_T=2, 6$, and 10 . Two crossings are visible for $\nu_T=10$, one for $\nu_T=6$, and none for $\nu_T=2$. Upper two curves are offset to align the expected crossing points. Filling of each layer given in (j,k) notation. (b) Landau level crossing diagram vs. D , features in (a) labeled by corresponding symbols. Solid lines, ML levels; dotted lines BL levels. The 0th ML LL is shown in red. The bilayer band gap $E_g(D)$ is indicated with a schematic dependence on D . For each D , the zero of energy is set at the center of the BL band gap. The fourfold degeneracy breaking is omitted for clarity.

References

- [1] A. Mishchenko, et al., *Nat. Nanotechnol.* **9**, 808 (2014).
- [2] R. Bistritzer and A. H. MacDonald, *Phys. Rev. B* **81**, 245412 (2010).
- [3] Y. Kim, et al., *Phys. Rev. Lett.* **110**, 096602 (2013).
- [4] C.-K. Lu and H. A. Fertig, *Phys. Rev. B* **89**, 085408 (2014).
- [5] A. M. van der Zande, et al., *Nano Lett.* **14**, 3869 (2014).
- [6] G. Li, A. Luican, and E. Y. Andrei, *Phys. Rev. Lett.* **102**, 176804 (2009).
- [7] B. Fallahazad, et al., *Nano Lett.* **15**, 428 (2015).
- [8] A. O. Sboychakov, A. L. Rakhmanov, A. V. Rozhkov, and F. Nori, *Phys. Rev. B* **92**, 075402 (2015).
- [9] P. Moon and M. Koshino, *Phys. Rev. B* **85**, 195458 (2012).
- [10] K. Liu, et al., *Nat. Commun.* **5**, 4966 (2014).
- [11] E. Suárez Morell, M. Pacheco, L. Chico, and L. Brey, *Phys. Rev. B* **87**, 125414 (2013).
- [12] J. D. Correa, M. Pacheco, and E. S. Morell, *J. Mater. Sci.* **49**, 642 (2013).
- [13] L.-J. Yin, J.-B. Qiao, W. Yan, R. Xu, R.-F. Dou, J.-C. Nie, and L. He, arXiv:1410.1621 [cond-mat] (2014).
- [14] C. R. Dean, et al., *Nature* **497**, 598 (2013).
- [15] L. A. Ponomarenko, et al., *Nature* **497**, 594 (2013).
- [16] B. Hunt, et al., *Science* **340**, 1427 (2013).
- [17] P. Wang, et al., *Nano Lett.* **15**, 6395 (2015).
- [18] H. Schmidt, J. C. Rode, D. Smirnov, and R. J. Haug, *Nat. Commun.* **5**, 5742 (2014).
- [19] J. D. Sanchez-Yamagishi, T. Taychatanapat, K. Watanabe, T. Taniguchi, A. Yacoby, and P. Jarillo-Herrero, *Phys. Rev. Lett.* **108**, 076601 (2012).
- [20] M. S. Dresselhaus and G. Dresselhaus, *Adv. Phys.* **51**, 1 (2002).
- [21] S. Kim, I. Jo, D. C. Dillen, D. A. Ferrer, B. Fallahazad, Z. Yao, S. K. Banerjee, and E. Tutuc, *Phys. Rev. Lett.* **108**, 116404 (2012).
- [22] L. A. Ponomarenko, R. Yang, R. V. Gorbachev, P. Blake, A. S. Mayorov, K. S. Novoselov, M. I. Katsnelson, and A. K. Geim, *Phys. Rev. Lett.* **105**, 136801 (2010).
- [23] A. H. Castro Neto, F. Guinea, N. M. R. Peres, K. S. Novoselov, and A. K. Geim, *Rev. Mod. Phys.* **81**, 109 (2009).
- [24] T. Taychatanapat, K. Watanabe, T. Taniguchi, and P. Jarillo-Herrero, *Nat. Phys.* **7**, 621 (2011).
- [25] Y. Lee, J. Velasco, D. Tran, F. Zhang, W. Bao, L. Jing, K. Myhro, D. Smirnov, and C. N. Lau, *Nano Lett.* **13**, 1627 (2013).
- [26] B. Partoens and F. M. Peeters, *Phys. Rev. B* **74**, 075404 (2006).
- [27] S. Latil and L. Henrard, *Phys. Rev. Lett.* **97**, 036803 (2006).
- [28] F. Guinea, A. H. Castro Neto, and N. M. R. Peres, *Phys. Rev. B* **73**, 245426 (2006).
- [29] Z. Ni, Y. Wang, T. Yu, Y. You, and Z. Shen, *Phys. Rev. B* **77**, 235403 (2008).
- [30] See Supplemental Material at <http://> for additional details.
- [31] Y. Zhao, P. Cadden-Zimansky, Z. Jiang, and P. Kim, *Phys. Rev. Lett.* **104**, 066801 (2010).
- [32] C. R. Dean, et al., *Nat. Nanotechnol.* **5**, 722 (2010).
- [33] E. A. Henriksen and J. P. Eisenstein, *Phys. Rev. B* **82**, 041412 (2010).
- [34] A. F. Young, et al., *Phys. Rev. B* **85**, 235458 (2012).
- [35] S. Luryi, *Appl. Phys. Lett.* **52**, 501 (1988).
- [36] J. P. Eisenstein, L. N. Pfeiffer, and K. W. West, *Phys. Rev. B* **50**, 1760 (1994).
- [37] M. Buttiker, *J. Phys.: Condens. Matter* **5**, 9361 (1993).
- [38] This gap accounts for the peak in R_{xx} observed in Fig. 1(b) near overall charge neutrality. Also, the gap is associated with a compensating density of states near the bilayer band edges that

leaves the relation between density and ϕ_b in eq. 1 nearly the same for sufficiently large doping.

- [39] P. Maher, et al., *Science* **345**, 61 (2014).
- [40] Y. Zhang, T.-T. Tang, C. Girit, Z. Hao, M. C. Martin, A. Zettl, M. F. Crommie, Y. R. Shen, and F. Wang, *Nature* **459**, 820 (2009).
- [41] E. V. Castro, K. S. Novoselov, S. V. Morozov, N. M. R. Peres, J. M. B. L. dos Santos, J. Nilsson, F. Guinea, A. K. Geim, and A. H. C. Neto, *Phys. Rev. Lett.* **99**, 216802 (2007).
- [42] D. C. Elias, et al., *Nat. Phys.* **7**, 701 (2011).